An Optimal Model-Based Control Technique to Improve Wind Farm Participation to Frequency Regulation

Francesco Baccino, *Student Member, IEEE,* Francesco Conte, *Member, IEEE,* Samuele Grillo, *Member, IEEE,* Stefano Massucco, *Senior Member, IEEE,* and Federico Silvestro, *Member, IEEE*

I. Introduction

THE CONTROL of the power grid is of primary importance, especially now that renewable energy sources (RESs) have widely spread. In fact, RESs may induce disturbances due both to their intrinsic randomness—although being partially predictable—and to possible structural weaknesses of the grid precisely where large RESs farms are connected to the grid [1]. National Regulating Authorities are asking inverter-interfaced power sources to sustain the grid during faults by implementing fault-ride-through capabilities [2]–[6]. Under this request lies the reasoning that this kind of player should not actively contribute to worsen grid conditions by disconnecting and, thus increasing the disturbances [7]. Large-scale wind farms (WFs) can contribute to move from this "passive" approach to an active paradigm, by offering a variation in the generated active power in order to help the grid to recover from under- and over-frequency conditions. Many control strategies have been proposed to achieve these results. Among the various aspects that can be dealt with, research has focused mainly on frequency support, especially by means of aggregate or synthetic inertial response. In [8], a probabilistic approach for the estimation of the aggregate inertial response of a WF is proposed. The authors state that the usual assumption of considering constant wind speeds during transients is inadequate and provides a method for estimating the aggregate inertial response of a WF, even though considering the same profile for each wind turbine. In [9], a centralized control approach is developed. Kinetic energy response is governed by traditional proportional integral (PI) controllers whose gains are varied in a fixed way during transients. Reference power signals for wind turbines are set to a constant large value for a preset discharge time (3 s) in order to let the wind turbines deliver their support. Subsequent recovery times are different for each wind turbine but are arbitrarily set before the transient occurs. Similarly, there is no dynamical adaptation of the behavior of each wind turbine. Moreover, the tuning of the gains of the PI controllers is critical and should involve a significant trial and error phase. A similar approach is shown in [10], where the main focus is to evaluate the amount of energy (i.e., active power) that a wind turbine can deliver for frequency support, especially in a hydro-dominated power system. In [11], the combination of droop control and inertia response is investigated for autonomous island systems with low overall inertia and lacking of interconnections. In [12], the response of wind turbines to frequency variation is studied using a single busbar model of the Irish transmission system. Frequency support is provided by means of droop governors and different technologies, and wind penetration scenarios have been investigated.

In [4] and [13], frequency support is achieved through the use of a high-pass filter (HPF). This can help to overcome one of the main problems of droop controllers, which require wind turbines to operate at derated conditions to provide steady-state contribution. The presence of a zero in the transfer function of the filter ensures that the filter itself does not give any contribution in steady-state operation. Nevertheless, some drawbacks can be highlighted. In fact, since the support action cannot be dynamically changed according to the operating conditions of the wind

Manuscript received November 29, 2013; revised April 24, 2014; accepted May 25, 2014. Date of publication July 01, 2014; date of current version June 17, 2015. Paper no. TSTE-00500-2013.

F. Baccino, F. Conte, S. Massucco, and F. Silvestro are with the Dipartimento di Ingegneria Navale, Elettrica, Elettronica e delle Telecomunicazioni, Università degli Studi di Genova, I-16145 Genova (GE) Italy (e-mail: francesco.baccino@unige.it; fr.conte@unige.it; stefano.massucco@unige.it; federico.silvestro@unige.it).

S. Grillo is with the Dipartimento di Elettronica, Informazione e Bioingegneria, Politecnico di Milano, I-20133 Milano, Italy (e-mail: samuele.grillo@polimi.it).

Color versions of one or more of the figures in this paper are available online.

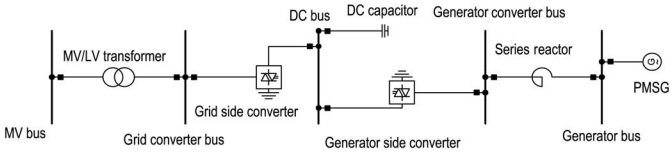

Fig. 1. Single line diagram of a full converter variable-speed wind generator.

turbines, the action that each controller can impose to a wind turbine must be suitably (i.e., in a conservative way) tuned in order not to make the wind turbines hit their operational limits whatever the initial conditions may be. In addition to this, the deactivation of the control is equally critical and suitable actions should be designed to avoid a fast change for the output power of the wind turbines.

In this paper, an optimal model-based approach is studied. The proposed control strategy exploits the model predictive control (MPC) approach [14], coupled with an estimation of the wind, for the definition of the contribution to frequency regulation of each wind generator. The main contribution of this paper is the combination of different techniques (i.e., KF and MPC) to estimate the variation in load and the actual operating conditions of each wind turbine and to define the optimal setpoint for each of them to effectively contribute to reduce frequency variation without hitting their operational limits. Moreover, the proposed approach has been tested in a software-in-the-loop framework.

This paper is structured as follows. In Section II, the implemented power system models (i.e., for aerogenerators, WF, and network) are outlined. In Section III, the designed control strategy, based on MPC theory, is described. It consists of a central controller, a central filter, and some local filters, one for each wind turbine. The central controller is disabled in normal operation conditions and its task is to set the power reference for each wind turbine, overwriting the local reference, when a disturbance occurs. Central KF is in charge of estimating the external load variation, while each local KF estimates wind speed and wind turbine's dynamical state. In Section IV, the simulation scenario and architecture are presented. Finally, in Section V, the obtained results are discussed.

II. Power System Model

The power system model is implemented in the DIgSILENT PowerFactory environment [15]. The model includes static and dynamic models for the components and the controllers.

A. Aerogenerator Model

The implemented wind generator model refers to a 2-MW full converter variable-speed wind turbine equipped with permanent magnet synchronous generator (PMSG), according to [16]. As described in Fig. 1, from left to right, the power system components that model the aerogenerator are an a medium voltage/low voltage (MV/LV) transformer, a grid-side power converter, a DC-link, a generator-side power converter, and a PMSG.

The wind generator dynamic model block diagram is depicted in Fig. 2. The models used for the synchronous machine and for the converters are the DIgSILENT built-in ones, while the models used for the wind, the aerodynamic, the drive train, the pitch control, the maximum power tracking (MPT) control, and

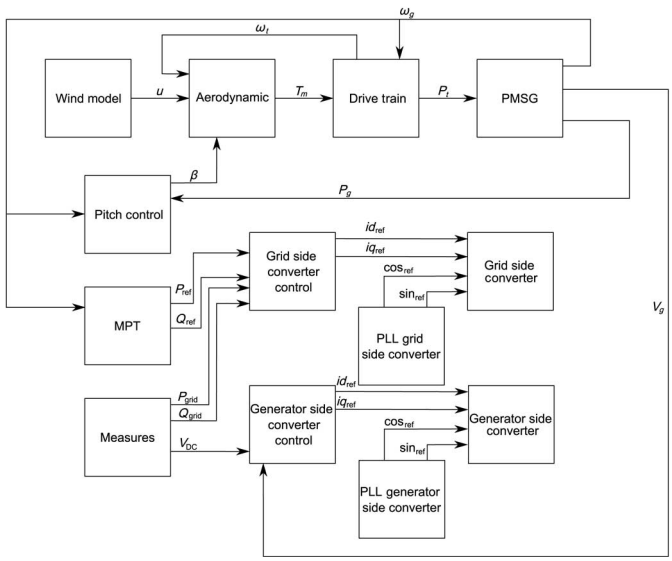

Fig. 2. Block diagram of the wind generator dynamic model.

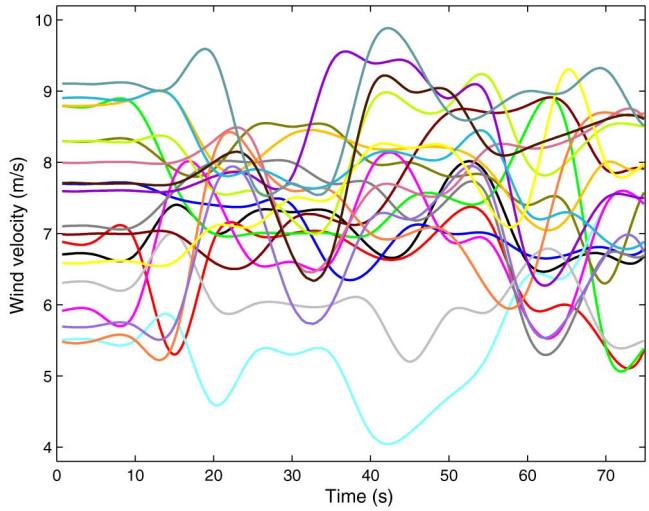

Fig. 3. Five-second-sampled wind profiles used in the simulations.

the converters controls have been implemented. There is a vast literature concerning the modeling of these systems and, as stated before, the main reference used in this work is [16]. In the following, some short notes about the implemented models are listed.

1) Wind Model: The wind profiles used in the simulations come from real measurements with 5-s sampling [17]. The data were statistically processed and sent to different machines after a spline interpolation. An example of the used wind profiles is depicted in Fig. 3.

2) Aerodynamic Model: The aerodynamic block computes the mechanical torque as a function of the wind speed, the pitch angle, and the rotational speed.

3) Drive Train Model: The drive train consists in a "soft" shaft and two masses that represent the generator and the rotor. This model is a tradeoff between the simplicity and ease of implementation and the need to picture oscillatory phenomena typical of this kind of applications and that cannot be neglected.

4) MPT Control: The MPT controller sends the active power set point to the grid-side converter control according to a lookup table that maps the maximum power for every generator speed.

5) Pitch Control: The pitch control acts in order to limit the rotor speed and the output power to the nominal values. It does so by modifying the aerodynamic efficiency of the blades.

6) Converters Control: The generator-side converter controls the voltage on the DC link and on the generator busbar. The grid-side converter controls the active and reactive power flows to the grid. During the normal operation, the active power set point comes from the MPT; whereas, during the frequency support, it is integrated with signals that depend on the frequency variation, and it will be discussed in the following. The reactive set point is fixed to zero, because in this work, the contribution of WFs to voltage support is not considered.

B. WF and Network Model

The implemented WF is composed of 20 wind generator dynamic models [wind turbine (WT)]. The turbines are located along four feeders, five turbines for each feeder. The turbines are connected by means of 1-km MV cables and two groups, ten machines in each group, that are connected to two 25 MVA $15/132$ kV/kV transformers by means of two 8-km MV cables. A 50-km overhead line connects the WF to the main grid which is represented by a load and a 1000 MVA plant. The plant is an equivalent model and is equipped with a steam turbine prime mover, frequency droop controller, and automatic voltage regulator (AVR). The adopted models are a classical IEEE steam turbine governor and a IEEE type 2 AVR. The models are characterized with the parameters listed in Tables I and II.

TABLE I
MAIN GRID EQUIVALENT GOVERNOR PARAMETERS

Concept	Symbol	Value	Unit
Turbine delay time constant	T_3	35.00	s
Turbine derivative time constant	T_2	10.00	s
Frictional losses factor	D_t	0.00	p.u.
Turbine power coefficient	A_t	1.00	p.u.
Controller droop	R	0.05	p.u.
Governor time constant	T_1	0.20	s

TABLE II
MAIN GRID EQUIVALENT AVR PARAMETERS

Concept	Symbol	Value	Unit
Measurement delay	T_r	0.02	s
Controller gain	K_a	100.00	p.u.
Controller time constant	T_a	0.03	s
Controller output maximum	$V_{\max}$	10.00	p.u.
Controller output minimum	$V_{\min}$	–10.00	p.u.
Exciter constant	K_e	1.00	p.u.
Exciter time constant	T_e	0.20	s
Stabilization path gain	K_f	0.05	p.u.
Stabilization path first time constant	T_{f1}	1.50	s
Stabilization path second time constant	T_{f2}	0.10	s
Saturation factor 1	E_1	3.90	p.u.
Saturation factor 2	S_{e1}	0.10	p.u.
Saturation factor 3	E_2	5.20	p.u.
Saturation factor 4	S_{e2}	0.50	p.u.

III. CONTROL STRATEGY

A. Output Tracking by MPC

The core of the control strategy proposed in this paper makes use of an MPC solution to the so-called *output tracking problem* [14], which is briefly recalled in this section.

The MPC is based on the knowledge of a time-domain model of the dynamical system to be controlled. In the formulation used in this paper, such a model has the linear discrete-time form

$$\boldsymbol{x}(k+1) = A\boldsymbol{x}(k) + B\boldsymbol{u}(k) + M\boldsymbol{d}(k) \tag{1a}$$

$$\boldsymbol{y}(k) = C\boldsymbol{x}(k) \tag{1b}$$

where $\boldsymbol{x}(k)$ is the state vector, $\boldsymbol{u}(k)$ is the control input, $\boldsymbol{d}(k)$ is the disturb vector, and $\boldsymbol{y}(k)$ is the output vector. The state $\boldsymbol{x}(k)$ and the disturb $\boldsymbol{d}(k)$ are supposed to be known at the time step k. The output tracking problem requires to determine the control $\boldsymbol{u}(k)$ in order to drive the output $\boldsymbol{y}(k)$ to follow a reference signal $\boldsymbol{y}^0(k)$. Within this formulation, the output matrix C is defined for selecting the state variables, which are required to follow the reference signal. For example, if C is the identity matrix, tracking will concern all state variables.

At the time step k, given a time horizon T and a control trajectory $\{\boldsymbol{u}(j); j = k, \ldots, k+T-1\}$, models (1a) and (1b) can be used to predict the evolution of the output signal $\boldsymbol{y}(k)$ over the time horizon. Therefore, once defined the tracking error as $\Delta\boldsymbol{y}(k) = \boldsymbol{y}(k) - \boldsymbol{y}^0(k)$, it is possible to determine the optimal finite horizon control trajectory $\{\boldsymbol{u}^*(k)\}$ by solving the following optimization problem:

$$\{\boldsymbol{u}^*(k)\} = \arg\min_{\{\boldsymbol{u}(k)\}} \sum_{j=k}^{k+T-1} \left(\|\Delta\boldsymbol{y}(j)\|_Q^2 + \|\boldsymbol{u}(j)\|_R^2 \right) + \|\Delta\boldsymbol{y}(T)\|_P^2 \tag{2}$$

s.t.

$$\boldsymbol{x}(k+1) = A\boldsymbol{x}(k) + B\boldsymbol{u}(k) + M\boldsymbol{d}(k) \tag{3a}$$

$$\boldsymbol{y}(k) = C\boldsymbol{x}(k) \tag{3b}$$

$$\boldsymbol{x}^{\min} \le \boldsymbol{x}(k) \le \boldsymbol{x}^{\max} \tag{3c}$$

$$\boldsymbol{u}^{\min} \le \boldsymbol{u}(k) \le \boldsymbol{u}^{\max} \tag{3d}$$

$$\Delta\boldsymbol{u}^{\min} \le \boldsymbol{u}(k) - \boldsymbol{u}(k-1) \le \Delta\boldsymbol{u}^{\max} \tag{3e}$$

where $\|\boldsymbol{v}\|_M^2 = \boldsymbol{v}^T M \boldsymbol{v}$. The positive definite matrices R, Q, and P in the cost function can be used to differently penalize the tracking error on the different output variables and the control energy. Constraints (3a) and (3b) allow the optimization to consider the model prediction. Constraints (3c)–(3e) can be used to assure the stability of the system and satisfy other control specifications (such as maximum control and maximum control rate).

Due to uncertainties in the system, such as model plant mismatches or errors on parameters, the optimal control trajectory $\{\boldsymbol{u}^*(k)\}$ does not result in the ideal system reaction

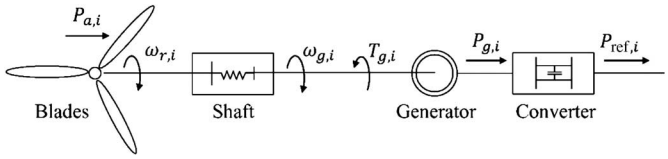

Fig. 4. Schematic representation of a full converter variable-speed wind turbine generator.

described by the system model at the end of the prediction horizon. To react to these problems, the idea of MPC is to introduce feedback by the receding horizon scheme, which consists in repeating the optimization at any time step k and apply the first element of the optimal control trajectory as the current control input, i.e., $\boldsymbol{u}(k) = \boldsymbol{u}^*(k)$. This assures a certain robustness with respect to parameters and model mismatches as a property of the feedback scheme, as it has been studied in [14]. One of the key features of MPC is the possibility to use an optimal control approach within a closed-loop scheme. This marks a difference from other model-based techniques. A further useful property is the possibility to introduce constraints. In some problems, these may allow the control to theoretically assure the system stability or to keep the system state within stability regions, established by external analyses.

B. Model Description

The models of the main system components used for designing an MPC-based control strategy are described in the following.

1) Variable-Speed Wind Turbines Generators Model: Consider a WF composed of N WTs. Each of them generally consists of an aeroturbine, a generator, and a full converter, as shown in Fig. 4. Hereafter, subscript i will indicate a quantity referred to the ith WT within the WF.

The aerodynamic power $P_{a,i}$ captured by the rotor of the aeroturbine is

$$P_{a,i} = \frac{1}{2}\rho\pi R^2 C_p(\beta_i, \lambda_i) v_i^3 \tag{4}$$

where ρ is the air density ($\mathrm{kg/m^3}$), R is the rotor radius (m), and v_i is the speed of the wind component perpendicular to rotor plane (m/s). The power coefficient C_p is the ratio between the available wind power and the power captured by the rotating blades. This coefficient depends on the blades' pitch angle β_i (deg) and the tip-speed ratio (TSR) λ_i, defined as

$$\lambda_i = \frac{\omega_{r,i} R}{v_i}$$

where $\omega_{r,i}$ is the blades' angular speed (rad/s). The power coefficient C_p depends on the aerodynamic characteristic of the blades' profiles. It usually derives from a collection of curves which indicate the aerodynamic efficiency as function of the TSR λ_i for fixed values of the pitch angle. However, it can be approximated by a fitting nonlinear function of λ_i and β_i [18], or, equivalently, of $\omega_{r,i}$, v_i, and β_i.

The aerodynamic power $P_{a,i}$ is transmitted to the generator by a shaft, whose dynamical behavior can be described with a two-masses model

$$\dot{\omega}_{r,i} = \frac{1}{J_r}\left(\frac{P_{a,i}}{\omega_{r,i}} - \mu\theta_{d,i} - \kappa\big(\omega_{r,i} - \omega_{g,i}\big)\right) \tag{5a}$$

$$\dot{\omega}_{g,i} = \frac{1}{J_g}\left(\mu\theta_{d,i} + \kappa\big(\omega_{r,i} - \omega_{g,i}\big) - \frac{P_{g,i}}{\omega_{g,i}}\right) \tag{5b}$$

$$\dot{\theta}_{d,i} = \omega_{r,i} - \omega_{g,i} \tag{5c}$$

where $\omega_{g,i}$ is the generator rotor angular speed (rad/s), J_r and J_g are the turbine and generator inertia ($\mathrm{kg\ m^2}$), respectively, $\theta_{d,i}$ is the shaft deformation angle (rad), μ is the shaft elastic constant ($\mathrm{kg\ m^2/s^2}$), and κ is the damping coefficient ($\mathrm{kg\ m^2/s}$).

The electro-mechanic torque $T_{g,i} = P_{g,i}/\omega_{g,i}$ directly depends on the generator power $P_{g,i}$ [W], which is delivered to the grid. The latter is determined by the power converter, which is driven by a reference signal $P_{\text{ref},i}$. The dynamic of the bridge converter is significantly faster than the mechanical one. Therefore, the converter is supposed to be ideal, so that $P_{g,i} = P_{\text{ref},i}$ [9], [19].

Finally, the total power delivered by the WF to the grid is

$$P_w = \sum_{i=1}^{N} P_{g,i}. \tag{6}$$

2) Power Network Primary Frequency Control Model: In the power network, the primary frequency control is generally operated by conventional generators which are required to keep the frequency close to the nominal value when power unbalances occur. The standard control strategy is known as *frequency droop control* by which the generators limit the frequency variation with a final droop $\Delta f/f^{\text{nom}} = -k_p(\Delta P/P^{\text{nom}})$, where ΔP is the grid power variation, k_p is the droop ratio, and f^{nom} and P^{nom} are the nominal frequency and power, respectively.

The relation between the power and frequency variations can be expressed in the Laplace domain as follows [20]:

$$\frac{\Delta f(s)}{\Delta P(s)} = -\frac{1}{k_f}\frac{\tau s + 1}{\frac{s^2}{\omega_n^2} + 2\frac{\zeta}{\omega_n}s + 1} \tag{7}$$

where k_f^{-1} is the steady-state gain ($k_f^{-1} = k_p f^{\text{nom}}/P^{\text{nom}}$). A possible approach for identifying the parameters of (7) is shown in [21]. By assuming the system stability, a state-space realization can be readily derived from (7) [22]

$$\dot{\Delta f} = \Delta f - a_1 x_f + b_1 \Delta P \tag{8a}$$

$$\dot{x}_f = -a_0 x_f + b_0 \Delta P \tag{8b}$$

where coefficients a_0, a_1, b_0, and b_1 directly depend on (7) and x_f is an auxiliary state variable.

By denoting the variation of the power delivered by the ith WT with $\Delta P_{g,i}$, the total grid power variation can be expressed as $\Delta P = \Delta P_L - \Delta P_w$, where $\Delta P_w = \sum_i \Delta P_{g,i}$ is the total variation of power provided by the WF and ΔP_L is the total external power load variation.

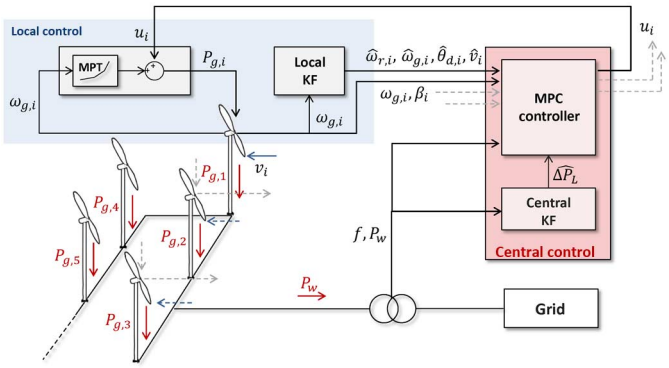

Fig. 5. Proposed control architecture.

C. Proposed Control Technique

The control structure proposed in this paper is depicted in Fig. 5. It consists of a *central controller* which receives the sampled measurements of the generators rotor angular speed $\omega_{g,i}$, the pitch angle β_i, the grid frequency variation Δf, and the total power delivered to the grid by the whole WF P_w.

The pitch angle control is independently determined by standard PI regulators which keep $\omega_{g,i}$ and $P_{g,i}$ under their nominal values ω^{nom} and P^{nom}. The WTs locally operate a conventional MPT regulation using a lookup table that defines the optimal power $P_{g,i}$ to be delivered to the grid for a given value of the measured rotor speed $\omega_{g,i}$, i.e., $P_{g,i} = P^*_{g,i}(\omega_{g,i})$. The mission of the central controller is to determine the variation u_i from the MPT signal in order to support the primary regulation when a significant frequency variation arises. The resulting control input for the ith WT is

$$P_{g,i} = P^*_{g,i}(\omega_{g,i}) + u_i. \tag{9}$$

The additive control signal u_i has to be computed by considering the wind conditions of each WT and guaranteeing the overall system stability. This is carried out through an MPC algorithm, which states the optimal tradeoff among the main control objective, which is the reduction of the frequency variation, and further specifications and/or system limitations.

As depicted in Fig. 5, the controller uses some estimated data (further than the mentioned direct measurements): 1) the estimated wind speeds $\hat{v}_i$; 2) the estimated dynamic state of the WTs $(\hat{\omega}_{r,i}; \hat{\omega}_{g,i}; \hat{\theta}_{d,i})$; and 3) the estimated total external power variation $\hat{\Delta} P_L$.

Wind speeds are required to adapt the control strategy to the local wind conditions of each generator. The dynamical state and the external load variation are required by the MPC which assumes to know the system state and to be provided by an estimate of unknown disturbances such as ΔP_L (see Section III-A).

The estimates of both the wind speeds and the dynamical states are computed by the WTs through a KF (local KF in Fig. 5). The external load variation is estimated by a unique KF (central KF in Fig. 5). The two estimation algorithms are first presented and followed by the description of the control algorithm.

1) Dynamical State and Wind Estimation Algorithm: Wind power generators are usually equipped with anemometers which provide a wind speed measurement. However, such data are not sufficiently accurate because of aerodynamic turbulent phenomena caused by the turbine rotating blades. Moreover, the wind measured by anemometers is not exactly equal to the component that transfers power to the aeroturbine rotors. Therefore, using direct wind measurements for estimation is not preferable.

The estimation must be carried out exploiting the indirect information given by the dynamical state of the considered WT which, as mentioned, is also required by the MPC algorithm. Wind and dynamical state estimations have to be computed by the same filtering procedure.

The main difficulties of this method are due to the nonlinear nature of the dynamical model (5a)–(5c) that requires the introduction of approximations. The relation between the dynamical state of the WTs and the wind speed is indeed given by the term $P_{a,i}$, which, in virtue of the power coefficient C_p [see (4)], depends on both the rotor angular speed $\omega_{r,i}$ and the same wind speed v_i, i.e., $P_{a,i} = P_{a,i}(\omega_{r,i}, v_i)$ (the dependence on β_i is omitted for convenience, since it is supposed to be available at any time).

Unfortunately, such a function is strongly nonlinear. This represents a double difficulty. Indeed, the filtering of nonlinear continuous-time systems with sampled measurements, requires the introduction of two approximations: 1) due to the use of zero-holding to discretize the state equations and 2) the linearization of both the state and output equations. Some literature approaches [23] propose a linear estimation of the aerodynamic torque $T_{a,i}$, followed by the numeric solution of the nonlinear equation $T_{a,i} = P_{a,i}(\omega_{r,i}, v_i)/\omega_{r,i}$. This may represent a drawback for real applications from the computational point of view. The idea of the filtering solution proposed in the following is to obtain a recursive estimation procedure and reduce as much as possible the significance of the above-mentioned approximations.

For each WT, the following state vector is defined

$$\boldsymbol{z}_i = \begin{bmatrix} \omega_{r,i} & \dot{\omega}_{r,i} & \omega_{g,i} & \theta_{d,i} & v_i \end{bmatrix}^T \tag{10}$$

which, considering (5a)–(5c), is governed by the dynamic model

$$\dot{z}_{i,1} = z_{i,2} \tag{11a}$$
$$\dot{z}_{i,2} = \sigma_\omega w_{i,1} \tag{11b}$$
$$\dot{z}_{i,3} = \frac{1}{J_g}\left(\kappa\left(z_{i,1} - z_{i,3}\right) + \mu z_{i,4}\right) - \frac{1}{J_g}\frac{P_{g,i}}{z_{i,3}} \tag{11c}$$
$$\dot{z}_{i,4} = z_{i,1} - z_{i,3} \tag{11d}$$
$$\dot{z}_{i,5} = \sigma_v w_{i,2} \tag{11e}$$

where $w_i \in \mathbb{R}^2$ is a standard zero-mean Gaussian white-noise process.

Two equations have been added with respect to (5a)–(5c). The former (11b) is the time derivative of the rotor angular acceleration $\dot{\omega}_{r,i}$ (sometimes called Jerk); the latter (11e) is the time derivative of the wind speed v_i. Both equations are supposed to be independent Gaussian white random processes with standard variations σ_ω and σ_v, respectively. Equation (11b) has been added in order to make the filter able to estimate the rotor angular acceleration. This allows the filtering process to use the rotor dynamical balance (5a) as an output equation, as shown in the following. This choice has been made for avoiding the

zero-holding of such a strongly nonlinear differential equation. Equation (11e) has been added in order to make the filter able to estimate the wind speed. Finally, the quantity $P_{g,i}$ is completely known by (9) and that the term $P_{g,i}/z_{i,3}$ constitutes the unique nonlinearity of the state equations (11a)–(11e).

Two measurements are, therefore, available for system (11a)–(11e). The first one is the generator angular speed $\omega_{g,i} = z_{i,3}$. The second one is the rotor dynamical balance (5a), which must be identically equal to zero. The output vector $\boldsymbol{y}_i = [y_{i,1}\ y_{i,2}]^T$ is, thus, composed by

$$y_{i,1} = \omega_{g,i} + n_{\omega_g,i}$$
$$y_{i,2} = n_{m,i}$$

where $n_{\omega_g,i}$ and $n_{m,i}$ are independent Gaussian white processes with standard deviations σ_{ω_g} and σ_m which model the measurement error of the generator angular speed and the model error in the dynamic balance (5a), respectively. The output vector $\boldsymbol{y}_i$ is related to the state vector (10) by the following output map:

$$y_{i,1} = z_{i,3} + n_{\omega_g,i} \tag{12a}$$
$$y_{i,2} = -\frac{1}{J_r}\left(\frac{P_{a,i}}{z_{i,1}} - \mu z_{i,4} - \kappa\big(z_{i,1} - z_{i,3}\big)\right) + z_{i,2} + n_{m,i} \tag{12b}$$

which is strongly nonlinear because of the term $P_{a,i}/z_{i,1}$.

The system described by (11a)–(11e) and (12a)–(12b) can be discretized by zero-holding, with sampling time T_s^f, which introduces approximations only for the presence of the forcing term $P_{g,i}/z_{i,3}$. The discretized model can be finally used to implement an estimation algorithm by applying the standard extended KF (EKF). The estimated state $\hat{z}_i$ will contain both the dynamical state of the considered WT $(\hat{\omega}_{r,i}; \hat{\omega}_{g,i}; \hat{\theta}_{d,i})$ and the wind speed $\hat{v}_i$.

The filtering procedure uses only local data. Therefore, it is reasonable to assume that this task is distributed to the WTs, if equipped with computing resources.

2) Total External Load Variation Estimation Algorithm: Model (8a)–(8b) can be rewritten and extended as follows:

$$\dot{\Delta f} = \Delta f - a_1 x_f + b_1 \Delta P_L - b_1 \Delta P_w \tag{13a}$$
$$\dot{x}_f = -a_0 x_f + b_0 \Delta P_L - b_0 \Delta P_w \tag{13b}$$
$$\dot{\Delta P_L} = w_{P_L} \tag{13c}$$
$$y_f = \Delta f + n_f \tag{13d}$$

where w_{P_L} and n_f are independent Gaussian white-noise processes, with standard deviation σ_{P_L} and σ_f, respectively, y_f is the available measurement, and ΔP_w is a completely known quantity. Since the resulting system is linear, it can be exactly discretized, with sampling time T_s^f and a standard KF algorithm can be used to estimate the state, which contains the required quantity ΔP_L. Obviously, since ΔP_w is known, the estimate $\hat{\Delta P} = \hat{\Delta P_L} - \Delta P_w$ is available as well.

3) Control Algorithm: The control consists of two tasks: 1) the *model update*, during which the system model is updated with a given sampling time T_s^{up} and no control variation is transmitted to the WTs (i.e., $u_i = 0\ \forall i = 1, 2, \ldots, N$) and 2) the *MPC frequency support* (MPC-FS), during which a proper MPC algorithm determines the contribution of each WT to the frequency control. These two tasks are detailed below, followed by the scheduling strategy (Section III-c) used for activating and deactivating the MPC-FS.

a) Model Update: The wind estimates, together with the direct measurements and the control input form (9), can be used to obtain a first-order approximation of the WT model (5a)–(5c). For each WT, the state variables are the variations $\delta\omega_{r,i}$, $\delta\omega_{g,i}$, and $\delta\theta_{d,i}$ from the steady-state values at which the linearization is computed. These variables are collected into the vector

$$\boldsymbol{x}_i = [\,\delta\omega_{r,i} \quad \delta\omega_{g,i} \quad \delta\theta_{d,i}\,]^T.$$

At any time, assuming the changes of the mean wind speed to be significantly slower than the mechanical dynamic, the steady-state values can be assumed to be $\bar{\omega}_{r,i} = \bar{\omega}_{g,i}$ equal to the measured $\omega_{g,i}$ and $\bar{\theta}_{d,i} = P^*_{g,i}(\bar{\omega}_{g,i})/(\mu\bar{\omega}_{g,i})$. Moreover, $\bar{\beta}_i$ is equal to the current measured β_i and $\bar{v}_i$ is assumed to be equal to the current estimate $\hat{v}_i$. The wind conditions data and the capability of a WT to support the frequency control and recover the optimal power delivery are considered by the linearized model through the aerodynamic and generator power derivatives computed at the "current" steady-state conditions

$$\left.\frac{\partial P_{a,i}}{\partial \omega_{r,i}}\right|_{(\bar{\beta}_i, \bar{\omega}_{r,i}, \bar{v}_i)}, \left.\frac{\partial P_{g,i}}{\partial \omega_{g,i}}\right|_{\bar{\omega}_{g,i}}.$$

Because of the control input (9), the variation of the total power provided by the WF ΔP_w assumes the following form:

$$\Delta P_w = \sum_{i=1}^{N} \Delta P_{g,i} = \sum_{i=1}^{N} \Big(P^*_{g,i}(\omega_{g,i}) + u_i - P^*_{g,i}(\omega^0_{g,i})\Big)$$

where $\omega^0_{g,i}$ is the generator angular speed at the control initialization. The last equation makes the power plant model (13a)–(13b) nonlinear with respect to $\omega_{g,i}$. Therefore, (13a)–(13b) must be linearized at $\overline{\Delta f} = 0$, $\bar{x}_f = 0$, and $\omega_{g,i} = \bar{\omega}_{g,i}$.

The linearized models of the WTs and the controlled grid frequency dynamic are finally included into a unique model with the following state and control vectors:

$$\boldsymbol{x} = \big[\boldsymbol{x}_1^T\, \boldsymbol{x}_2^T \cdots \boldsymbol{x}_N^T\, \delta f\, \delta x_f\big]^T \tag{14a}$$
$$\boldsymbol{u} = [u_1\, u_2 \cdots u_N]^T. \tag{14b}$$

Such a model gives a complete representation of the dynamics of all the quantities to be controlled. After a zero-hold discretization, with sampling time T_s^c, the model can be rewritten in the standard discrete-time linear form (1a). In this case, the disturb vector $\boldsymbol{d}(k)$ actually is equal to the scalar quantity ΔP_L at the sampling time kT_s^c. Note that the filtering procedures described in Sections III-C1 and III-C2 provide the estimates of both the state $\boldsymbol{x}(k)$ and the disturb $\boldsymbol{d}(k)$. Equation (1a) is the model to be updated at any time step kT_s^{up}.

b) MPC Frequency Support (MPC-FS): After the discretization, the MPC solution reported in Section III-A can be used to solve the main problem of this work. The

interest is to support the frequency control with a short-term action ($\sim 10 \div 60$ s), maintaining secure conditions and recovering the optimal power delivery after the support phase. In the particular case of this work, the controlled variables selected by the mapping $\boldsymbol{y}(k) = C\boldsymbol{x}(k)$ in (1b) are all state variables except for δx_f, which has not physical meaning. The reference signal $\boldsymbol{y}^0(k)$ is identically equal to zero for the dynamical WTs' states.

As far as the frequency reference signal is concerned, in nominal conditions, the equilibrium point to be reached should be $\Delta f = 0$. However, when a power unbalance occurs, the primary frequency control is asked to drive the frequency variation to the droop $\Delta f = -k_p(\Delta P/P^{\text{nom}})f^{\text{nom}}$ (see Section III-B2). This means that the condition $\Delta f = 0$ cannot be reached in short term. In fact, it will be reached by the secondary frequency control within a longer time interval. The support provided by the WF must be activated only for a short time ($\sim 50 \div 80$ s), i.e., the control action must have the same 0-type behavior of the frequency droop control. To attribute this behavior to the MPC controller, the frequency reference signal is dynamically set to $\Delta f^0 = -k_p(\Delta\hat{P}/P^{\text{nom}})f^{\text{nom}}$, where the estimate $\Delta\hat{P}$ is provided by the central KF described in Section III-C2.

The positive definite matrices R, Q, and P in the cost function (2) are used to differently penalize the tracking error on the wind speeds, the tracking error on the grid frequency, and the control energy.

The following constrains are introduced to assure structural stability and secure operational conditions:

$$\omega_r^{\text{cut-in}} \leq \omega_{r,i} \leq \omega^{\text{nom}} \tag{15a}$$
$$\omega_r^{\text{cut-in}} \leq \omega_{g,i} \leq \omega^{\text{nom}} \tag{15b}$$
$$-\theta_d^{\max} \leq \theta_{d,i} \leq \theta_d^{\max} \tag{15c}$$
$$0 \leq u_i + P^*(\omega_{g,i}) \leq P^{\text{nom}} \tag{15d}$$
$$-\Delta P^{\max} \leq u_i(k) - u_i(k-1) \leq \Delta P^{\max} \tag{15e}$$

where $\omega_r^{\text{cut-in}}$ is the cut-in angular speed, $\theta_d^{\max}$ is the maximal shaft torsion, and $\Delta P^{\max}$ is the maximum control variation. Constraints (15a)–(15c) allow the control to keep the WTs into their region of stability. Moreover, constraint (15d) limits the power delivered by the WF under the rated power and constraint (15e) regulates the control variation.

c) Scheduling Strategy: When $|\Delta f - \Delta f^0|$ is lower than a given *activation threshold* $\Delta f_{\text{th}}^{\text{a}}$, the only model update is active. When the quantity $|\Delta f - \Delta f^0|$ crosses the activation threshold, the MPC-FS control is activated. When $|\Delta f - \Delta f^0|$ becomes lower than the *deactivation threshold* $\Delta f_{\text{th}}^{\text{d}} < \Delta f_{\text{th}}^{\text{a}}$, the frequency support is turned OFF. The use of a double threshold strategy allows the control system to avoid chattering and sharp control variations.

IV. Simulations

The control technique proposed in Section III is implemented as MATLAB code and then tested and validated in a simulated field implemented within the DIgSILENT Powerfactory [15] environment as described in Section II.

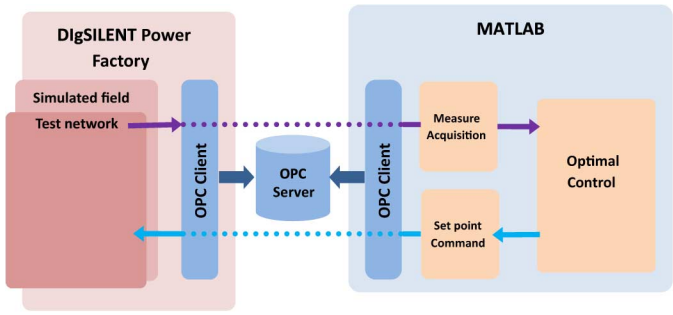

Fig. 6. Communication architecture.

TABLE III
MPC Parameters

Concept	Symbol	Value	Unit
Control sampling time	T_s^c	1	s
Filtering sampling time	T_s^f	0.2	s
Update sampling time	T_s^{up}	1	s
Activation threshold	Δf_{th}^a	0.1	Hz
Deactivation threshold	Δf_{th}^d	0.025	Hz
MPC prediction horizon	T	8	—
MPC control horizon	—	8	—

For every wind turbine, the grid-side converter control manages the power injections toward the grid on the base of the MPT signals. The generator-side converter control keeps the voltage constant at the generator busbar and the dc busbar. The pitch control acts limiting the speed and the power production. The wind profiles in input to the simulations are derived from real measurements and statistically processed in order to obtain different profiles for the different turbines.

The communication between the DIgSILENT-simulated field and the MATLAB MPC controller is realized through an Object Linking and Embedding (OLE) for Process Control (OPC) link as depicted in Fig. 6. Both DIgSILENT and MATLAB have in fact the capability to act as OPC clients, able to read and write on an OPC server. The tags of the signals of interest have to be coherently defined on the server and the clients. Thus, they can be read and written with the OPC methods.

Table III reports the main parameters of the control algorithm.

In order to evaluate the advantages of the proposed technique, the idea of kinetic energy control adopted in [4] and [13] is considered as a benchmark strategy. In these works, the wind power delivery is temporarily changed as response to a frequency variation through the use of a HPF. In the context of this paper, this is equivalent to substitute the MPC control signals u_i with the following law:

$$u_i(s) = -\frac{a_1 s}{b_2 s^2 + b_1 s + b_0}\Delta f(s) \quad \forall i = 1, 2, \ldots, N. \tag{16}$$

As mentioned also in [13], the HPF $F(s)$ has to be tuned carefully. In the under-frequency case, there is indeed a risk of reducing the rotating speed of the machines too much, which would force them out of the stable operating range. Therefore, the law (16) is included within the DIgSILENT model. The resulting signal $P_{g,i}$ in (9) is limited under the nominal power P^{nom}.

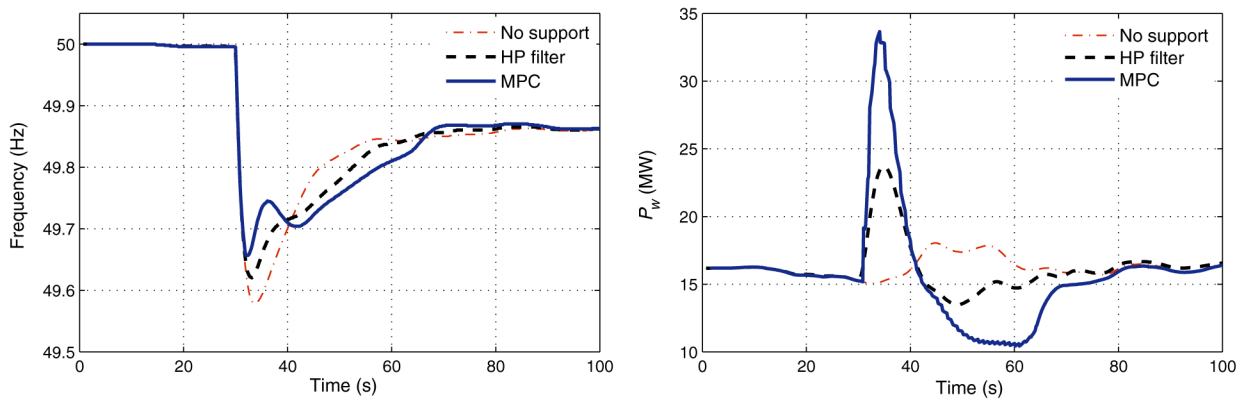

Fig. 7. Simulation results. (a) Grid frequency without frequency support of the WF (dotted–dashed orange), with the MPC-FS (solid blue), and with the HPF-FS (dashed black). (b) Corresponding total power delivered by the WF.

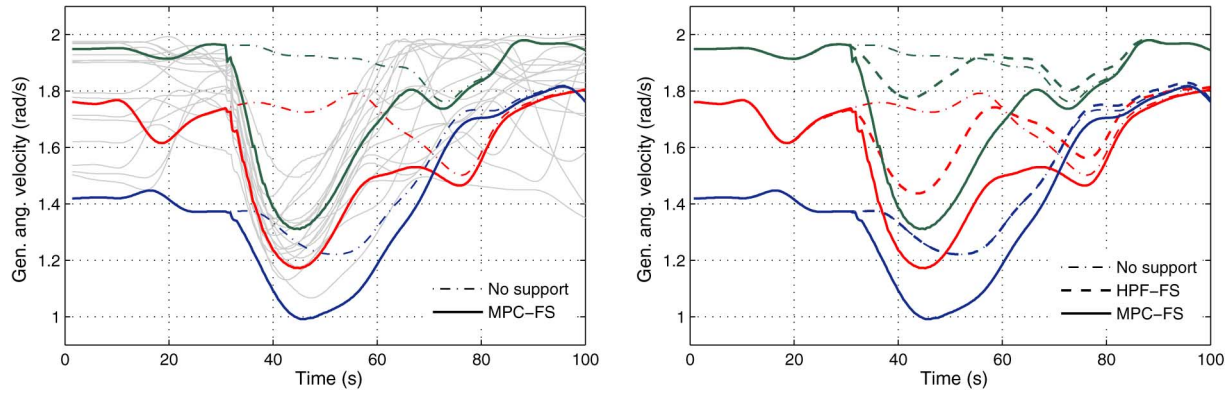

Fig. 8. Simulation results. (a) Generators angular speeds $\omega_{g,i}$ of 20 WTs in the case of activation of the MPC-FS. The speeds of three particular WTs are emphasized. For these three WTs, the generator angular speeds are also reported in the case without frequency support with dotted–dashed lines. (b) Comparison of the three emphasized generator angular speeds in the cases without frequency support (dotted–dashed), with MPC-FS (solid), and with HPF-FS (dashed).

Moreover, in order to avoid that the WTs with low speeds exit from the stable operating range, the HP filter is disabled under a certain threshold $\omega^d_{\rm th}$. The parameters used in the simulations are $a_1 = 650,\ b_0 = 1,\ b_1 = 10,\ b_2 = 20,$ and $\omega^d_{\rm th} = 1.6$ rad/s. These values have been defined in order to optimize the contribution of the WF to the frequency regulation in the considered scenario. In the following, this control strategy will be referred to as HPF frequency support (HPF-FS).

V. Results

Figs. 7–9 show the simulation results obtained in the wind conditions introduced in Fig. 3 (average speeds between 5 and 10 m/s). At 30 s, an external over-load of 50 MW occurs. The primary frequency control operated by the main grid is immediately activated as well as the MPC-FS operated by the WF. Figs. 7–9 also report the results obtained with the HPF-FS described in Section IV.

Fig. 7(a) shows that the MPC-FS succeeds in limiting the frequency variation more than the HPF-FS. The minimum value reached without frequency support is equal to 49.58 Hz. With the MPC-FS and the HPF-FS, the minimum values are 49.66 Hz (reduction of the 19%) and 49.62 Hz (reduction of the 9.5%), respectively. A similar difference can be found also in Fig. 7(b) where the powers delivered by the whole WF in the three cases are reported. The limitations on the variations of frequency is obtained by MPC-FS and HPF-FS through a short-term increase

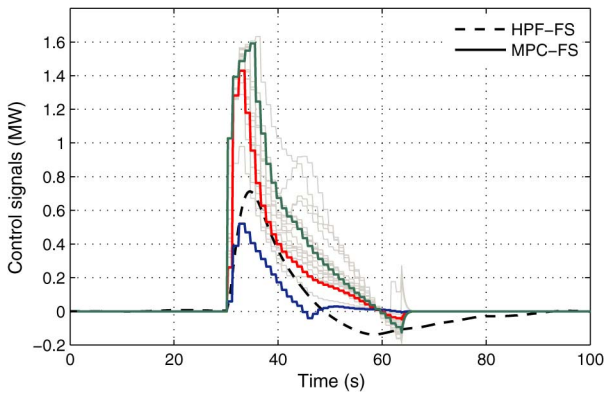

Fig. 9. Simulation results. Control signals u_i of the MPC-FS (solid) and the unique control signal of the HPF-FS (dashed). The emphasized MPC control signals are referred to the same WTs considered in Fig. 8.

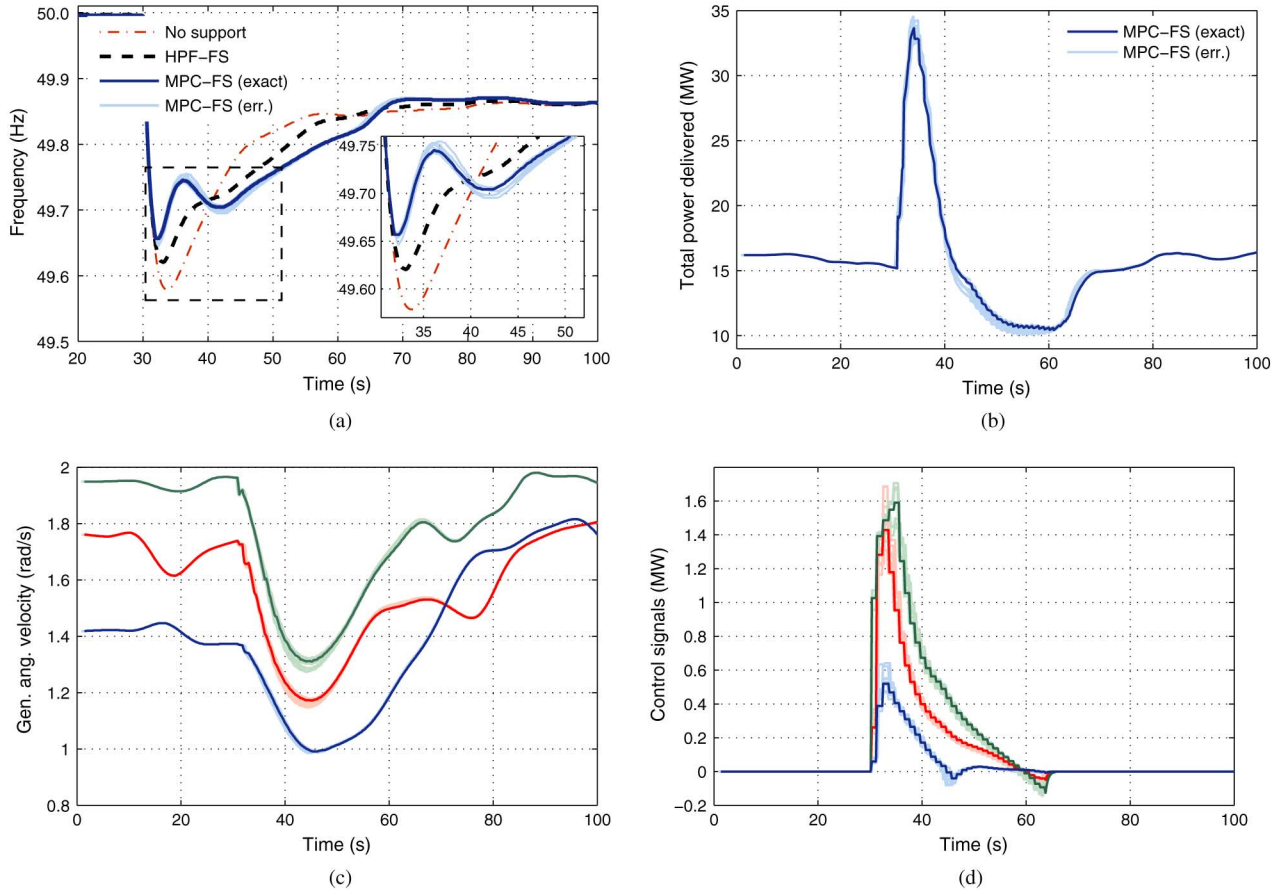

Fig. 10. Robustness analysis. (a) Grid frequency obtained with the MPC-FS with exact parameters (solid dark blue) and with the eight cases of erroneous parameters (solid clear blue). The frequency obtained without frequency support (dotted–dashed orange) and with the HPF-FS (dashed black) are also reported. (b) Corresponding total power delivered by the WF with exact and erroneous parameters. (c) and (d) Generator angular speeds $\omega_{g,i}$ and the MPC control signals u_i of the three WTs emphasized in Figs. 7 and 9, respectively. In both figures, dark colors refer to the case of activation of the MPC-FS with exact parameters, whereas clear colors refer to the eight cases with erroneous parameters.

of the power delivery. It is evident that in the case of MPC-FS, the power variation is significantly higher with respect to the case of HPF-FS.

Figs. 8 and 9 give an explanation to the above-mentioned results. In all these figures, the signals referred to three selected WTs are emphasized for clarity of presentation. Fig. 9 depicts different MPC control signals, compared with the unique control signal of the HPF. The consequent variations of the generators angular speeds $\omega_{g,i}$ are depicted in Fig. 8.

Fig. 8(a) reports the case of MPC-FS. When the over-load occurs, all speeds decrease, allowing the WF to deliver more power in about 10 s. After this phase, speeds increase toward the values determined by the MPT lookup table. Such an acceleration is obtained by the lower power delivery which is occurring at the same time. Consider now the three emphasized WTs. When the over-load occurs, they have different angular speeds: the green one is the fastest, the red one is the medium, and the blue one is the slowest. This is obviously due to different wind conditions because of the use of the MPT control. If compared with the dash-dotted lines, which depict the corresponding speeds in the case without frequency support, it is clear that the speed variations are similar for the fastest and medium cases, and lower in the slowest case. The similarity between the two first WTs means that the MPC operates the expected coordination of the aeroturbines. In fact, the deceleration of the faster WTs is obtained with a higher power delivery, as shown in Fig. 9. In other words, the MPC demands more power to the faster WTs, which have a larger kinetic energy reserve. For slower WTs, the deceleration is further limited since the rotor speed is too much close to the cut-in speed. This behavior is remarkable since it is due to the introduction of the constraint $\omega_r^{\mathrm{cut-in}} \leq \omega_{g,i} \leq \omega^{\mathrm{nom}}$, which is one of the key properties of the proposed MPC approach.

Fig. 8(b) compares the generator angular velocities of the three selected WTs in the case without frequency support and with MPC-FS and HPF-FS. The first and third cases coincide for the slower WT (blue) which is under the threshold ω_{th}^d. The variation determined by the HPF-FS is significantly lower than the one of MPC-FS, in particular for the fastest WT (green). This is due to the fact that the control signal of the HPF-FS shown in Fig. 9 is the same for all WTs. Therefore, it requires to be moderated in order to avoid that some of the slower turbines reach the cut-in speed. The result is that the potential power variation available from the faster turbines is not completely used, differently from what happens with the MPC-FS.

In order to analyze the robustness of the MPC-FS with respect to errors in the parameters of the control model (5a)–(5c), the simulation presented in Figs. 7–9 is repeated using different

(erroneous) parameters with respect to the simulated field. The attention is focused on the damping coefficient κ, the shaft elastic constant μ, and the turbine inertia J_t. The value used in the field model are $\kappa = 2 \cdot 10^6$ kg m^2/s, $\mu = 10^7$ kg m^2/s^2, and $J_t = 6 \cdot 10^6$ kg m^2. Eight simulations are carried out introducing $\pm 5\%$ errors to these values within the 2^3 possible combinations.

Fig. 10 shows the results of such simulations. No significant variation on the results occurs, especially for the generator angular velocities depicted in Fig. 10(c). This means that the stability of WTs is not compromised. Regarding the frequency, shown in Fig. 10(a), the limitation of the minimum always is better than the one obtained by the HPF-FS.

Finally, it is worth mentioning that by repeating the simulations with variations on parameters of 10% and 20%, the stability of the WTs is still kept.

VI. Conclusion

This paper presents a model-based control technique to improve the contribution of wind power generators to primary frequency regulation in electric power systems. The control technique is based on an MPC approach and on a Kalman-like estimation algorithm for the wind speed of each wind turbine. This leads to a centralized control which is able to adapt the control signals in an optimal way for each wind turbine. Optimality is achieved by minimizing a cost function subject to a set of constraints which define a physically consistent operating area. The results, obtained from a simulated field made up of 20 wind generators, show the feasibility and the effectiveness of the proposed approach. A robustness analysis has been carried out in order to test the dependency of the proposed approach to model parameters. Due to its intrinsic nature, based on the estimation of the dynamical state of each wind turbine, the control strategy proved to be suitably resilient.

References

[1] J. Lin, Y. Sun, Y. Song, W. Gao, and P. Sørensen, "Wind power fluctuation smoothing controller based on risk assessment of grid frequency deviation in an isolated system," *IEEE Trans. Sustain. Energy*, vol. 4, no. 2, pp. 379–392, Apr. 2013.

[2] C. Rahmann *et al.*, "Justified fault-ride-through requirements for wind turbines in power systems," *IEEE Trans. Power Syst.*, vol. 26, no. 3, pp. 1555–1563, Aug. 2011.

[3] G. Ramtharan, A. Arulampalam, J. Ekanayake, F. Hughes, and N. Jenkins, "Fault ride through of fully rated converter wind turbines with AC and DC transmission," *IET Renew. Power Gener.*, vol. 3, no. 4, pp. 426–438, Dec. 2009.

[4] S. Grillo *et al.*, "Transient support to frequency control from wind turbine with synchronous generator and full converter," in *Proc. 45th Int. Univ. Power Eng. Conf. (UPEC)*, Sep. 2010, pp. 1–6.

[5] D. Xiang, L. Ran, P. Tavner, and S. Yang, "Control of a doubly fed induction generator in a wind turbine during grid fault ride-through," *IEEE Trans. Energy Convers.*, vol. 21, no. 3, pp. 652–662, Sep. 2006.

[6] L. G. Meegahapola, T. Littler, and D. Flynn, "Decoupled-DFIG fault ride-through strategy for enhanced stability performance during grid faults," *IEEE Trans. Sustain. Energy*, vol. 1, no. 3, pp. 152–162, Oct. 2010.

[7] L. Xie *et al.*, "Wind integration in power systems: Operational challenges and possible solutions," *Proc. IEEE*, vol. 99, no. 1, pp. 214–232, Jan. 2011.

[8] L. Wu and D. G. Infield, "Towards an assessment of power system frequency support from wind plant—Modeling aggregate inertial response," *IEEE Trans. Power Syst.*, vol. 28, no. 3, pp. 2283–2291, Aug. 2013.

[9] P.-K. Keung, P. Li, H. Banakar, and B. T. Ooi, "Kinetic energy of wind-turbine generators for system frequency support," *IEEE Trans. Power Syst.*, vol. 24, no. 1, pp. 279–287, Feb. 2009.

[10] N. R. Ullah, T. Thiringer, and D. Karlsson, "Temporary primary frequency control support by variable speed wind turbines—Potential and applications," *IEEE Trans. Power Syst.*, vol. 23, no. 2, pp. 601–612, May 2008.

[11] I. D. Margaris, S. A. Papathanassiou, K. D. Hatziargyrou, A. D. Hansen, and P. Sørensen, "Frequency control in autonomous power systems with high wind power penetration," *IEEE Trans. Sustain. Energy*, vol. 3, no. 2, pp. 189–199, Apr. 2012.

[12] G. Lalor, A. Mullane, and M. O'Malley, "Frequency control and wind turbine technologies," *IEEE Trans. Power Syst.*, vol. 20, no. 4, pp. 1905–1913, Nov. 2005.

[13] I. Erlich and M. Wilch, "Primary frequency control by wind turbines," in *Proc. IEEE Power Energy Soc. Gen. Meet.*, Jul. 2010, pp. 1–8.

[14] D. Mayne, J. Rawlings, C. Rao, and P. Scokaert, "Constrained model predictive control: Stability and optimality," *Automatica*, vol. 36, pp. 789–814, 2000.

[15] *DIgSILENT PowerFactory User's Manual*, version 15.0. Gomaringen, Germany: DIgSILENT GmbH.

[16] A. Hansen *et al.*, "Dynamic wind turbine models in power system simulation tool DIgSILENT," RisÃ¸ Nat. Lab., Tech. Univ. Denmark, Roskilde, Denmark, Tech. Rep. Risø-R-1400(EN), Aug. 2007.

[17] S. Grillo, M. Marinelli, S. Massucco, and F. Silvestro, "Optimal management strategy of a battery-based storage system to improve renewable energy integration in distribution networks," *IEEE Trans. Smart Grid*, vol. 3, no. 2, pp. 950–958, Jun. 2012.

[18] H. Ma and B. Chowdhury, "Working towards frequency regulation with wind plants: Combined control approaches," *Renew. Power Gener. IET*, vol. 4, no. 4, pp. 308–316, Jul. 2010.

[19] N. van Deelen, A. Joki, P. van den Bosch, and R. Hermans, "Exploiting inertia of wind turbines in power network frequency control: A model predictive control approach," in *Proc. IEEE Int. Conf. Control Appl.*, Sep. 2011, pp. 1309–1314.

[20] F. Saccomanno, *Electric Power Systems: Analysis and Control*. Hoboken, NJ, USA: Wiley-IEEE Press, 2003.

[21] C. Bruno *et al.*, "An innovative pluralistic load-frequency control scheme for the power flow control along corridors on the Italian border," in *Proc. IEEE Power Syst. Conf. Expo. PSCE*, Oct. 2006, pp. 2166–2173.

[22] W. J. Rugh, *Linear System Theory*, T. Kailath, Ed. Englewood Cliffs, NJ, USA: Prentice Hall, 1996.

[23] W. Qiao, W. Zhou, J. Aller, and R. Harley, "Wind speed estimation based sensorless output maximization control for a wind turbine driving a DFIG," *IEEE Trans. Power Electron.*, vol. 23, no. 3, pp. 1156–1169, May 2008.